

# Strain analysis based on EAM and applications on surface, vacancy, and boundary of Al\*

Shigeto R. Nishitani<sup>†</sup>

*Department of Informatics, Kwansei Gakuin University.*

(Dated: April 8, 2024)

Stress or strain analysis for each atom around structural defects in a crystal is difficult. We propose a new analytical approach based on the eminent Embedding Atom Method(EAM) potential. We observe that the ratio  $R$  between the repulsive and binding terms of the EAM is a definite measure for calculating the strain field of a single atom subject to an irregular coordination number. The determination of adequate potential parameters and their application to the calculation of the properties of surface, vacancy, and boundary of pure Al are shown.

## I. INTRODUCTION

Geometrical phase analysis (GPA) is an innovation in the area of materials science, and has been improved over the past few decades[1]. This novel method allows us to describe the exact strain fields that are present around dislocations by utilizing high resolution TEM images or atomistic simulations[2, 3]. When the coordination numbers of the atoms around a dislocation change, it is not trivial to understand its compression or expansion behaviors.

The other classical method, the Voronoi polygon analysis[4], is suitable in this case, because it involves easier calculations for changes in the coordination number. In this method, a polygon is well defined by the surrounding atoms. However, for a vacancy or a surface, the volume of a specific atom can not be well defined. In fact, the subsequent atoms might be too far away, or infinitely distant, due to these structural defects.

The atomistic simulations performed by calculations based on first principles provide reliable values for the positions of the atoms and the total energy of the system. However, precise stress or energy value of each atom is hardly obtained. Rigorous efforts have been dedicated to establishing the atomic size dividings of the total values based on the first principles calculations [5, 6]. The difficulty of this approach is rooted in the ambiguity of dividing the wave functions in the real space.

In order to avoid these difficulties, we propose a new analytical approach based on the eminent Embedding Atom Method(EAM) potential. We propose that the ratio  $R$  between the repulsive and binding terms of the EAM is a definite measure for calculating the strain field per atom even with the altered coordination numbers. In this paper, we first recall the EAM potential method, especially with the applied first nearest neighbor model. Secondly, we compare the structural energies and equilibrium distances of different perfect lattices and observe how the changes in coordination number affect the EAM potential. Subsequently, we discuss the fitting of the

EAM potential for a suitable prediction of the strain field in different systems. Finally, we observe a few examples of the strain field analysis of the EAM on the defect structures in pure aluminum, such as surface, vacancy, and boundary.

## II. RATIO BETWEEN REPULSIVE AND BONDING ENERGIES

The embedded atom method (EAM) was developed for metals by Daw and Baskes[7]; this method essentially considers each metal atom to be embedded within an electron density field generated by the surrounding atoms:

$$E_{\text{total}} = E_{\text{repulsive}} - E_{\text{bond}} = \sum \phi_{ij} - F(\rho), \quad (1)$$

where  $\phi_{ij}$  is the simple pair repulsive interaction between  $i - j$  atoms, and  $\rho$  is the electron density of the field. When we take  $F(\rho) = \sqrt{\rho}$  and we express the electron density with the following equation defined by hopping integrals  $h(r_{ij})$ ,

$$\rho = \sum h(r_{ij})^2,$$

we can obtain the Finnis-Sinclair potential[8]; this potential is equivalent to the one obtained by the second-moment models of Ducastelle [9]. This second-moment approximation limits the identification of the differences in structural energy between hcp and fcc structures[10, p.223]. Higher moment models of bond order potentials, including the angular dependence on bonding, show different tendencies for the values of the structural energies depending on the dimension of the lattices [11]; herein, the three-dimensional structures are always more stable than the two- or one-dimensional structures. Among the three-dimensional structures, the dependence of cohesive energy on the equilibrium distance between two atoms primarily shows the same trend as that in the second moment models. Because the targets in this paper are the defects in three dimensional lattices, we settled to a second moment approximation.

We introduce two more constraints to simplify the analysis. First, we select a simple exponential function

\*

<sup>†</sup> nishitani@kwansei.ac.jp; <https://ist.ksc.kwansei.ac.jp/~nishitani>

for the pair and the hopping interactions as follows,

$$\phi(r_{ij}) = a_0 \exp(-pr_{ij}) \quad (2)$$

$$h(r_{ij}) = b_0 \exp(-qr_{ij}) \quad (3)$$

where  $r_{ij}$  is the inter-atomic distance between  $i$  and  $j$  atoms. The coefficients  $a_0$  and  $b_0$  are usually determined by the equilibrium condition. The structural energy is simply determined by the  $p/q$  ratio, where fcc structure is more stable than diamond structure for  $p/q > 2$ , and diamond is more stable than fcc for  $p/q < 2$  [11].

Second, we consider only the first nearest neighbor interaction. We observe that the ratio between  $E_{\text{repulsive}}$  and  $E_{\text{bond}}$  is a constant at its equilibrium distance and is independent of the coordination number  $n$ . When we consider a perfect lattice with the identical inter-atomic distance, the total energy per atom can be simply given as

$$\begin{aligned} E_{\text{total}} &= \sum a_0 \exp(-pr) - \sqrt{\sum b_0^2 \exp(-2qr)} \\ &= na_0 \exp(-pr) - b_0 \sqrt{n \exp(-2qr)}. \end{aligned} \quad (4)$$

The first derivative of distance  $r$  of this equation is as follows;

$$\frac{dE_{\text{total}}}{dr} = -npa_0 \exp(-pr) + qb_0 \sqrt{n \exp(-2qr)} \quad (5)$$

The solution of the note of this equation gives the equilibrium distance  $r_n$  for a coordination number of  $n$ , and gives the following relation;

$$\frac{qb_0}{pa_0 \sqrt{n}} = (\exp(q-p))^{r_n}. \quad (6)$$

Calculating the ratio  $R$  between  $E_{\text{repulsive}}$  and  $E_{\text{bond}}$ , we obtain the following:

$$R = \frac{E_{\text{repulsive}}}{E_{\text{bond}}} = \frac{na_0 \exp(-pr_n)}{b_0 \sqrt{n \exp(-2qr_n)}} \quad (7)$$

$$= \sqrt{n} \frac{a_0}{b_0} \left( \frac{\exp(q)}{\exp(p)} \right)^{r_n} \quad (8)$$

Now, substituting  $r_n$  from eq.(6) will result in the following relation,

$$R = \sqrt{n} \frac{a_0}{b_0} \frac{qb_0}{pa_0 \sqrt{n}} = \frac{q}{p} \quad (9)$$

which is independent of the coordination number.

This relation holds correctly for the perfect lattices, such as those cases when  $n = 12, 8, 6$ , and  $4$ , which correspond to fcc, bcc, simple cubic and diamond structures, respectively. It is also valid for imperfect lattices, such as those cases where  $n = 11, 10, 9, 7, 5, 3, 2$ , and  $1$ . Thus, the ratio  $R$  will be a measure of the strain field around a single atom; this is true for any environment consisting of different coordination numbers, as shown in the next section in detail.

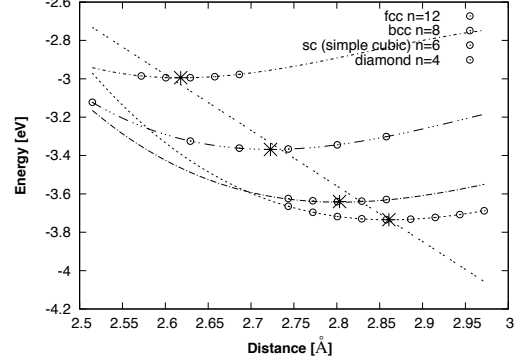


FIG. 1. Structural energy and minimum positions for the perfect lattices of Al obtained by the first principles calculations.

### III. FITTING TO THE FIRST PRINCIPLES CALCULATION RESULTS

Empirical potentials are fitted to the physical properties of real materials, and one easy way is to use the first principles calculation results for this fitting procedure. The target of this study is to characterize the strain field for structures with different coordination numbers. Thus, the structural energies obtained from the first principle calculations are the starting point for the fitting of the EAM.

Figure 1 shows the dependence of structural energy on the inter-atomic distance, and the values corresponding to the minimum positions for the perfect lattices of Al obtained by the first principles calculations with the coordination number  $n = 12, 8, 6$  and  $4$  for fcc, bcc, sc (simple cubic) and diamond, respectively. The calculation conditions are as follows: To begin with, the first principles calculations are performed by VASP (Vienna ab initio simulation package)[12], implementing PAW (Projector Augmented Wave)[13] and GGA (Generalized Gradient Approximation)[14] for the calculations of pseudo potentials, and the default energy cut off for the plane wave. The  $k$ -point mesh used in each calculation was automatically generated by VASP, because the cell sizes depend on the perfect lattices. For this automatic generation, the length parameter defined in VASP was set to 100 after checking for energy convergence.

The first principles calculation results show the clear tendency of a decrease in inter-atomic distance with decreasing coordination numbers[11]. The minimum values for distance and energy show a nearly linear relation. The straight line plotted in Fig. 1 is calculated by the least square fit passing through the minimum position of the fcc lattice. In the bcc lattice, the second nearest neighbors are the closest in comparison to the other structures; however, this feature is not obvious from this plot and will be discussed later.

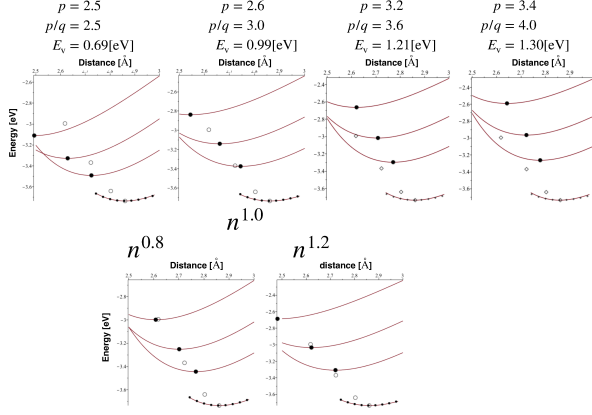


FIG. 2.  $p/q$  dependency of the equilibrium points on the structural energy (open circles), with the first principles calculations (solid circles).

The explicit expression of the EAM potentials is shown in eq.(4) where  $n$  denotes the coordination number, and  $a_0$  and  $b_0$  are determined from the equilibrium condition, the cohesive energy and the equilibrium distance.  $p$  and  $q$  define the distance dependence of the potentials, and are determined from the curvature of the structural energy function and correspond to the bulk modulus. The ratio  $p/q$  determines the stable points of the structures as shown in Figs. 2.

Firstly, we set  $p/q$  to be 2.5 and  $p$  was determined by the bulk modulus of the fcc structure. Based on these values, the stable points for bcc, sc and diamond can be determined. The slope of the line connecting the stable points will increase as the  $p/q$  value increases. The vacancy formation energy is also related to the  $p/q$  values, and this relation is illustrated in Figs. 2, where an increase in the  $p/q$  ratio results in an increase in the vacancy formation energy.

Taking a power of the coordination number, such as  $n^{0.8}$  or  $n^{1.2}$ , the stable points can be fitted more closely to the results obtained from the first principles. From the technical point of view of simulations, this effect is not calculated from the surrounding sites, but is usually included through the embedding function  $F(\rho)$  in Eq.(1). Because the change in this function alters the final result of the dependence of coordination on the ratio between bonding and repulsive energies that were obtained, as stated in the previous section, we don't adopt a power of the coordination number.

The parameters,  $p = 3.2$  and  $p/q = 3.6$ , are the adopted values used in the rest of the paper, whose equilibrium points for different coordination numbers are shown in Fig.3. The equilibrium points are not close to those of first principles results shown in the same figure. The reason for the selection of these parameter values is explained as follows.

Table I shows the comparison of the structural energy

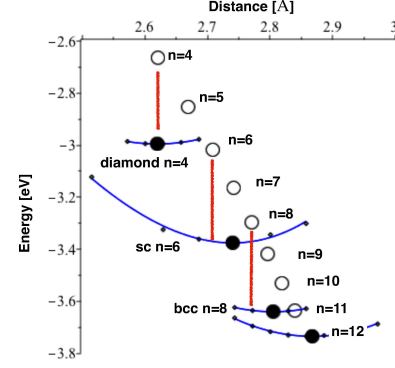


FIG. 3. The equilibrium point change for different coordination numbers (open circles), with the structural energies obtained by first principles calculations (solid circles).

TABLE I. Comparison of the energy and distance values between predictions by the EAM and values by the first principles calculations.

structure	energy and distance	EAM potential	first principle
bcc	energy [eV]	-3.2967	-3.6397
	distance [Å]	2.7707	2.8032
Simple cubic	energy[eV]	-3.0174	-3.3681
	distance [Å]	2.7084	2.7226
Diamond	energy [eV]	-2.6635	-2.9943
	distance [Å]	2.6207	2.6179
Vacancy formation	energy [eV]	1.21	0.7

and, inter-atomic distances obtained with the EAM prediction with the selected parameters, and the first principles calculations. For the case of the diamond lattice, the energy of -2.6635 eV is obtained by EAM; this value is significantly different from -2.9943 eV, which is obtained by the first principles calculations, while the inter-atomic distance from the EAM, 2.6207 Å, is close to the first principles value of 2.6179 Å. The probability of this trend between discrepancies and similarities is the same for the other structures as well. The minimum point for bcc structure is significantly different from those for the other structures; this is reasonable because the EAM potential neglects the interactions farther than the first nearest neighbors, which are relevant and should be included for bcc structures. Because the surrounding atoms around mono-vacancy in fcc structure have the coordination number of 11, the vacancy formation energies should be related to those systems with coordination number of 11, and are also much different. Because the aim of applying the EAM potential in this research is not for energy assessment but for strain analysis, we therefore selected the parameters which better reproduce accurate inter-atomic distances rather than energy values.

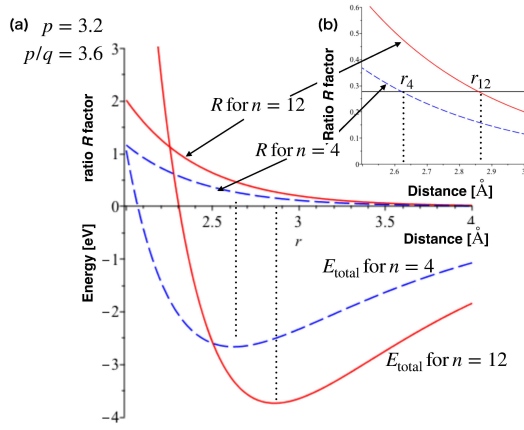


FIG. 4.  $E_{\text{total}}$  and  $R$  dependency on distance for  $n = 12$  (fcc) and 4 (diamond). The inset figure (b) gives a closer view around the equilibrium distances and  $R$  dependencies.

Figure 4 shows the  $E_{\text{total}}$  and  $R$  dependency on the distance for coordination numbers  $n = 12$  (fcc) and 4 (diamond). The inset figure (b) gives a closer view around the equilibrium distances and  $R$  trends. At each equilibrium distance of  $r_{12} = 2.8584$  and  $r_4 = 2.6207$  Å for fcc and diamond, respectively, the ratios  $R$  show the same value of 0.27778, which is the inverse of  $p/q$ . At the minimum distance for the other coordination numbers,  $R$  shows the same value as expected by the theoretical derivations. Furthermore, the distance dependence of  $R$  for each coordination number shows a monotonous dependency to the inter-atomic distance. Thus  $R$  is a good measure for the strain fields; a compressing field is observed for  $R > 0.27778$  and an expanding field is observed for  $R < 0.27778$ . We will see the applications of this measure around some lattice defects in the next section.

#### IV. APPLICATIONS ON DEFECTS

The defects we focus on in this section are surface, vacancy, and boundary, in pure aluminum. The configurations for these defects are obtained by the automatic ionic relaxations of VASP with the parameters described in the previous section.

##### A. Surface relaxations

Figure 5 shows the relaxation trends for (100), (110) and (111) surfaces. Figure 5(a) shows a traditional plot of the inter-layer spacing dependencies to the distance of the layers from the surface. We can compare them to the experimental and calculated results summarized by Rodriguez *et al*[15]. The inter-layer spacing is depicted as a % of the inter-layer spacing of a perfect lattice depending on the marks of the first-second, second-third inter-layer

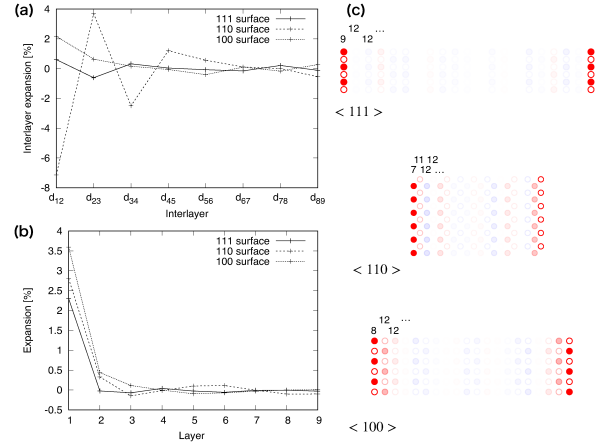


FIG. 5. Strain field diagrams for surfaces displaying (100), (110) and (111) surfaces; (a) inter-layer spacing, (b) strain field analysis and (c) strain field representation using colors of different intensities.

spacing  $d_{12}$ ,  $d_{23}$  and so on. A typical behavior of Al surface relaxation is observed in the (110) surface, where a 10% contraction of the first inter-layer and a 5% expansion of the second inter-layer are observed both in experiments and calculations. Conversely, the first inter-layer of the (100) and (111) surfaces in experiments and calculations show the scattered results of small positive or negative values. The results of our study show the expansions in both surfaces; however, the values are small.

Comparing to the variable trends in the inter-layer spacing plots, our strain field analysis shows an identical behavior on the relaxations of the different surfaces of Al. Figure 5 (b) shows the expanding distances calculated from the relations displayed in Figs.4 using the value  $R$  from the EAM. All atoms in the first layer expand about 2 to 4% in all surfaces, while the atoms in the second layer behave differently for different surfaces. Although the atoms of the second layer in the (111) surface shows approximately no change in the absence of the strain field, those in the (100) and (110) surfaces remain in the expanding positions. The oscillating behavior shows a different tendency in (111), (100) and (110) surfaces. In the (111) surface, the oscillation of the strain field drops quickly after the first layer, and very small oscillation is observed in the third layer. Alternatively, for the (100) and (110) surfaces, the oscillations are preserved until the fourth and fifth layers.

These significantly different dependencies between the strain field and the inter-layer distances, as seen in Figs.5(a) and (b), are explained by the differences in coordination number. The coordination numbers of each layer are shown in the small characters on the left side of Fig.5(c); (9,12,12,...), (7,11,12,12,...), and (8,12,12,...) for (111), (110), and (100) surfaces, respectively. We set the cut off distance between the first and the second nearest neighbor sites, which is clearly determined for each surface. When we change the measure from the distance

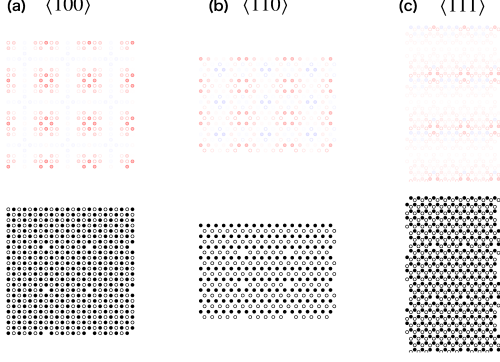


FIG. 6. Visual display of the strain field around vacancy.

to the ratio  $R$ , the expansion or compression magnitudes begin to depend on the coordination number. The large compression of the first inter-layer of the (110) surface becomes an expansion for the atoms with a coordination number of 7. The oscillatory behavior observed in the inter-layer distances damps quickly; the expansion and compression are only observed in those layers with the coordination numbers different from 12 or just below.

The three plots in Figs.5(c) show the color coded representations of the expansion-compression plots highlighting the magnitude for every atom; red and blue represents expansion and compression, respectively, and the brightness of the color represents the magnitude of these behaviors. The open and closed circles represent the upper and lower layers along the direction perpendicular to the sheet. The (111) surface shows a bright red color in the first layer, whereas it shows a very pale colors for the atoms below the second layer. The (110) and (100) surfaces show red colored atoms in the second layer also, whereas they show very pale colors below the third layer. These representations are sufficient to grasp the expansion-compression field and its magnitude.

The values of the strain can be compared with the stresses obtained by the first principles analysis of Shihara *et al*[5]. Their estimation of the stresses on the (111) surface of Al comprises a large expansion for the first layer, which is consistent with the results of this study. On the other hand, for the second layer, they predicted an in-plane compression, and its magnitude is about one third of that of the first layer. This oscillatory behavior in stress is rooted on the difficulty of the dividing of the spaces around the different coordination numbers.

### B. Vacancy relaxations

Figures 6 show visual representations of the strain field for the vacancy. Each column shows the cutting direc-

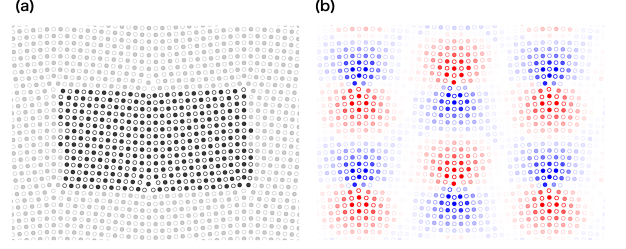


FIG. 7. Visual representation of the strain field display for boundaries, (a) for a relaxed atom configuration and (b) a color coded strain field representation.

tion, and the first and the second layers intersecting vacancies are shown with the open and closed circles, respectively. The first nearest atoms around the vacancy show an expanding behavior as same as in the surface. An oscillatory behavior, on the other hand, cannot be observed in any sectioning planes around the vacancy. This result is consistent with the results obtained from the first principles calculation[6]; the first site around the vacancy shows a large expanding stress, however, the other sites show nearly zero stress.

### C. Boundary relaxations

Figures 7 show the strain fields around the  $\langle 100 \rangle$  symmetric tilt grain boundary with an angle of  $7.63^\circ$ . Figure 7(a) shows a unit cell and its surroundings with high and low contrasts, respectively. The boundaries are located vertically on the center and on both sides of the unit cell for which the periodic conditions are applied. The open and closed circles represent the upper and lower layers along  $[001]$  axis. We can recognize the dislocations at equidistant positions along the boundaries.

Figure 7(b) is a visual representation of the strain using  $R$  in the EAM analysis, where the color and color brightness of each site mean the same as that in Figs.5(c) and Figs.6. The region between the boundaries shows a pale color, which indicates small strain as for a perfect lattice. On the other hand, boundary regions are represented with an intense color. The centers of the blue and red pairs are located at the dislocations and the round shapes of these cells show the typical shape of strain fields around dislocations of the Peierls-Nabarro dislocation model [3].

Figures 8 shows (a) 3d, (b) vertical and (c) lateral plots of the strain field values. The 3d parse view of Fig.8(a) shows a unit cell, where large deviations from the perfect

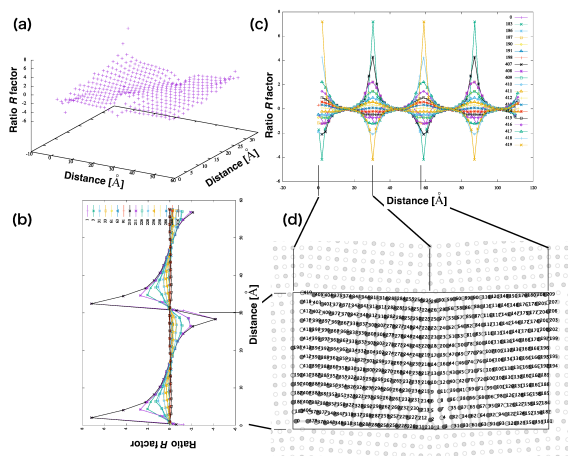


FIG. 8. (a) 3d, (b) vertical and (c) lateral plots of the strain field values calculated from the ratio  $R$  for boundaries. (d) shows the indexing for the atoms.

lattice are observed around the dislocations located at the boundary. The vertical view along the boundary of Fig.8(b) shows periodic peak and valley pairs. Following the atom indexes as shown in Fig.8(d), No.1 and No.210 are located at the center bottom of the unit cell. As shown in Fig.8(b), the lines pass through the maximum value of the expanding field at No.2, and decrease to the minimum value, indicating a very large compression at No.29. When we observe the lateral plots in Fig.8(c), No.419 is located at the right end of the upper most line, and shows the largest expanding strain due to the surrounding configurations. When the line moves right to the center of the unit cell, the strain changes from expansion to compression, and hits a minimum at No.29. We can observe a smooth shifting of the strain field with changes in the coordination number; for No.2, the dislocation core has  $n = 10$ , No.1 and No.210 also have

$n = 10$ , whereas No.3 and No.211 have  $n = 11$ . No.4 and No.213 show different coordination numbers of 10 and 12, respectively, due to the slight asymmetry of the relaxed configuration. However, they show nearly identical values for the strain field. This means that the slight difference of the coordination number does not affect significantly on the strain field values calculated from the  $R$  factor of the EAM.

## V. CONCLUSIONS

We have derived a measure of the strain field from EAM potentials. The ratio  $R$  between the repulsive energy and the bonding energy for single atoms shows the same value at the minimum point for different coordination numbers  $n$ ; these values were calculated under some approximations applied to the EAM potential including using the square root function of the electron density, the exponential dependency on the repulsive and hopping interactions, and for the calculation of the first nearest neighbor interactions. We have shown the applications of this novel method on the surface, vacancy, and boundary of pure Al. For each atom around these defects, having altered coordination numbers, the expanding or compressing strain calculated from the  $R$  factor of the EAM shows the smooth change, which is expected from continuum mechanics.

## VI. ACKNOWLEDGEMENT

The author thanks to Mr. Shunji Nishitani, who showed the derivation of Eq.(9) for the first time. This work was carried out using the JFRS-1 supercomputer system at Computational Simulation Centre of International Fusion Energy Research Centre (IFERC-CSC) in Rokkasho Fusion Institute of QST (Aomori, Japan).

- 
- [1] M. Hÿtch, E. Snoeck, and R. Kilaas, "Quantitative measurement of displacement and strain fields from hrtem micrographs," *Ultramicroscopy*, vol. 74, pp. 131–146, 1998.
  - [2] M. J. Hÿtch, J.-L. Putaux, and J.-M. Pénisson, "Measurement of the displacement field of dislocations to 0.03 Å by electron microscopy," *Nature*, vol. 423, pp. 270–273, 2003.
  - [3] Z. Dong and C. Zhao, "Measurement of strain fields in an edge dislocation," *Physica B*, vol. 405, pp. 171–174, 2010.
  - [4] G. Voronoi, "Nouvelles applications des paramtres continus la thorie des formes quadratiques. premier mmoire. sur quelques proprits des formes quadratiques positives parfaites," *J. reine angew. Math.*, vol. 133, pp. 97–178, 1908.
  - [5] Y. Shiihara, M. Kohyama, and S. Ishibashi, "Ab initio local stress and its application to al (111) surfaces," *Phys. Rev. B*, vol. 81, p. 075441, 2010.
  - [6] H. Wang, M. Kohyama, S. Tanaka1, and Y. Shiihara, "Ab initio local energy and local stress: application to tilt and twist grain boundaries in cu and al," *J. Phys.: Condens. Matter*, vol. 25, p. 305006, 2013.
  - [7] M. S. Daw and M. I. Baskes, "Embedded-atom method: Derivation and application to impurities, surfaces, and other defects in metals," *Phys. Rev. B*, vol. 29, p. 6443, 1984.
  - [8] M. W. Finnis and J. E. Sinclair, "A simple empirical n-body potential for transition metals," *Phil. Mag. A*, vol. 50, pp. 45–55, 1984.
  - [9] F. Ducastelle, "Modules lastiques des mtaux de transition," *J. de Physique*, vol. 31, p. 11, 1970.
  - [10] D. G. Pettifor, *Bonding and structure of molecules and solids*. Clarendon Press(Oxford), 1995.
  - [11] S. R. Nishitani, P. Alinaghian, C. Hausleitner, and D. G. Pettifor, "Angularly dependent embedding poten-

- tials and structural prediction,” *Phil. Mag. Lett.*, vol. 69, pp. 177–184, 1994.
- [12] G. Kresse and J. Hafner, “Ab initio molecular dynamics for liquid metals,” *Phys. Rev. B*, vol. 47, pp. 558–61, 1993.
  - [13] G. Kresse and D. Joubert, “From ultrasoft pseudopotentials to the projector augmented-wave method,” *Phys. Rev. B*, vol. 59, pp. 1758–75, 1999.
  - [14] J. P. Perdew and Y. Wang, “Accurate and simple analytic representation of the electron-gas correlation energy,” *Phys. Rev. B*, vol. 45, pp. 13244–9, 1992.
  - [15] A. M. Rodríguez, G. Bozzolo, and J. Ferrante, “Multilayer relaxation and surface energies of fcc and bcc metals using equivalent crystal theory,” *Surf. Sci.*, vol. 289, pp. 100–126, 1993.